Organic Electronics 13 (2012) 593–598

Contents lists available at SciVerse ScienceDirect

Organic Electronics

journal homepage: www.elsevier.com/locate/orgel

Self-assembled monolayer modification of silver source–drain electrodes for high-performance pentacene organic field-effect transistors

Hui-Yu Chen [a], I-Wen Wu [a], Chin-Ti Chen [b], Shun-Wei Liu [b,c,*], Chih-I Wu [a,*]

[a] Department of Electrical Engineering and Graduate Institute of Photonics and Optoelectronics, National Taiwan University, Taipei 10617, Taiwan, ROC
[b] Institute of Chemistry, Academia Sinica, Taipei 11529, Taiwan, ROC
[c] Department of Electronic Engineering, Mingchi University of Technology, New Taipei City 24301, Taiwan, ROC

ARTICLE INFO

Article history:
Received 26 July 2011
Received in revised form 17 November 2011
Accepted 31 December 2011
Available online 13 January 2012

Keywords:
Photoemission
TFT
Organic
Pentacene

ABSTRACT

We demonstrated excellent performance improvement of bottom-contact pentacene-based organic thin film transistors (OTFTs) fabricated at room-temperature with silver electrodes modified by self-assembled monolayers (SAMs) of binary mixtures of *n*-alkanethiol (*n*-decanethiol, HDT) and the fluorinated analog (3,3,4,4,5,5,6,6,7,7,8,8,9,9,10,10,10-heptadecafluoro-1-decanethiol, FDT). The OTFTs with modified silver (Ag) electrodes exhibit carrier mobility of 0.21 cm^2/V s, which is faster than most of bottom-contact pentacene-based OTFTs fabricated at room-temperature with gold (Au) electrodes. The threshold voltage is reduced from −30 V of the devices with Au electrodes to −5.4 V of the devices with modified Ag electrodes. The hole injection barrier is also reduced with modified Ag as indicated by ultraviolet photoemission spectroscopy. The enhancement of the saturation current and the mobility of the devices are due to both the reduction of hole injection barriers and the continuous grain size of pentacene on top of electrodes and dielectrics.

1. Introduction

Organic thin film transistors (OTFTs) have attracted great attention due to their prominent advantages, such as the potential for low-cost productions, easy fabrications, flexibility with substrates, and low temperature processing procedures [1–4]. Numerous electronic devices based on the OTFT, such as driving circuits for organic light-emitting diodes (OLEDs), radio frequency identification (RFID) tags, and sensors were reported [5–7]. The bottom-contact (BC) configuration of OTFT is suitable for integrated circuit applications, because the photolithography method can be applied in the fabrication process. For the top-contact (TC) OTFT, organic semiconductor layers can be damaged during the metal photolithography process. Thus, implementing the bottom contact structure is important for device fabrication and process integration. For this reason, a lot of research efforts have been focusing on BC-OTFT to achieve comparable performance as that of TC-OTFT.

In organic thin film transistors, the device performance is not only dependent on the intrinsic electrical properties of the organic semiconductors, but is also governed by the interfaces between the electrodes and the organic semiconductors [8–11]. The crucial factor at the interface is the injection barrier, which is determined by the energy difference between the work function of electrodes and the highest occupied molecular orbital (HOMO) level of the organic semiconductors. Therefore, gold (Au) with a relatively high work function of ~5.1 eV, which matches the HOMO energy level of most p-type organic semiconductors, has been commonly applied as source/drain (S/D) electrodes to lower the injection barrier [12–14]. However, due to the difficulty of etching and high cost problem associated with Au, an alternative metal for S/D electrodes is required. Silver (Ag) is one of the candidates, which has the highest conductivity of all metals and lower cost than gold. In addition, the work function of Ag also can be tuned by self-assembled monolayers (SAMs) [15,16].

* Corresponding authors.
E-mail addresses: swliu@mail.mcut.edu.tw (S.-W. Liu), chihiwu@cc.ee. ntu.edu.tw (Chih-I Wu).

1566-1199/$ - see front matter © 2012 Elsevier B.V. All rights reserved.
doi:10.1016/j.orgel.2011.12.016

The electrical performance of OTFTs with SAM-modified Au electrodes has been reported [17–19]. Several works has attributed that the reduction of injection barrier is a major factor leading to the improved performance of OTFTs [20–22]. Others reported that the improvement resulted from the morphological effects of SAMs modified electrodes [18,23].

However, the effect of SAM-modified Ag has not been deeply investigated. In this report, we demonstrated the bottom-contact organic thin film transistors with mixed SAMs of *n*-alkanethiol (*n*-decanethiol, HDT) and its fluorinated analog (3,3,4,4,5,5,6,6,7,7,8,8,9,9,10,10,10-heptadecafluoro-1-decanethiol, FDT) on silver electrodes, which have the work function tuned to be comparable with Au electrodes. The *n*-alkanethiol serves to decrease the work function and the fluorinated thiol is known to increase the work function of the substrates [17]. Varying the composition of these two SAMs could tune the work function of silver to desirable values [16]. The pentacene TFTs with SAM-modified Ag electrodes exhibited a good threshold voltage lower to −5.4 V. Enhancements of electrical characteristics, in both saturation current and carrier mobility, were achieved. To in depth investigate the mechanisms of enhancements, the electronic structures and the morphology of SAM-modified electrodes were also studied via UV photoemission spectroscopy (UPS) and atomic force microscopy (AFM).

2. Experimental

The pentacene thin films were deposited in our laboratory-designed thermal vacuum chamber equipped with the in situ electrical characterization measurements. The electrical measurements on the OTFT devices were performed in situ under high vacuum condition to achieve a precise threshold voltage (V_{th}), drain current, carrier mobility (μ), and on/off ratio.

The silver substrates were prepared by thermally evaporating 50 nm of silver on silicon wafer covered with a thick layer (300 nm) of thermally grown SiO_2. The Ag substrates were immersed in a 1 mM ethanolic solution of thiol mixtures consisting of FDT and HDT with 3:1 mol ratio for 0.5 h [16]. The substrates were then rinsed with acetone and dried with N_2 flow before being transferred into deposition chamber. FDT and HDT were purchased from Aldrich. The bottom-contact devices were fabricated with heavily doped silicon wafer with a 300 nm thick layer of thermally grown SiO_2 on top (C_i = 12 nF/cm^2). The oxide layer serves as the gate insulator and heavily doped silicon substrates is the gate electrode. The Si wafer was ultrasonically cleaned in acetone and isopropanol for 10 min, and then was etched in a piranha solution (70 vol.% H_2SO_4:30 - vol.% H_2O_2) for 30 min, and finally rinsed in D.I. water. Before deposition of pentacene, silver and gold electrodes (50 nm) were patterned through shadow masks at a rate 0.1 nm/s by thermal evaporation. Silver electrodes were then immersed in a 1 mM ethanolic solution of binary mixtures of thiols for 30 min. Pentacene films (50 nm) were evaporated with a deposition rate of 0.03 nm/s on the Au and Ag electrodes modified by SAMs in our laboratory-designed in situ electrical measurement setup with a base pressure around 8×10^{-6} [24]. The substrates were kept at room temperature during pentacene deposition.

The electrical measurements were performed by a semiconductor parameter analyzer (Keithley 2636), with electrical contacts to devices inside the vacuum chamber. Photoemission experiments were performed in two interconnected ultrahigh-vacuum chambers, one for deposition and one for spectroscopy analysis. The valence bands were investigated via UPS with a He discharge lamp, which provides both He I (21.2 eV) and He II (40.8 eV) photon lines as excitation sources. Morphological characterization was carried out by AFM (noncontact mode; Park system XE-100). The substrates were prepared exactly the same ways as those for the transistors.

3. Results and discussion

The work function of silver electrodes can be tuned by two SAMs (HDT and FDT) by varying the ratio of the mixtures. The work function of silver electrodes modified by various mole ratios of SAMs (HDT and FDT) is shown in Fig. 1. The measurement of work function was conducted by photoelectron spectrometer (AC-2 from Riken Keiki). The work function of silver was measured to be 4.26 eV. As shown in Fig. 1, for single-component HDT modified silver electrodes, the work function is about 4.3 eV; and for single-component FDT modified silver electrodes, the work function is about 6.0 eV. Using binary mixtures of these two SAMs in various molar ratios, the work function of silver electrodes can be tuned between 4.3 eV and 6.0 eV. Since the active layer of the TFT in this study has the ionization energy of about 5.2 eV, FDT:HDT mixture with 3:1 ratio was used to modify the Ag electrode in order to align the Fermi level to the lowest unoccupied molecular orbital (LUMO) of pentacene.

The drain current–drain voltage characteristics of pentacene TFT with bare gold electrodes, gold and silver electrodes modified by mixtures SAMs are shown in Fig. 2a–c, respectively. As the drain voltage (V_D) increases, the linear and saturation regions can be observed with

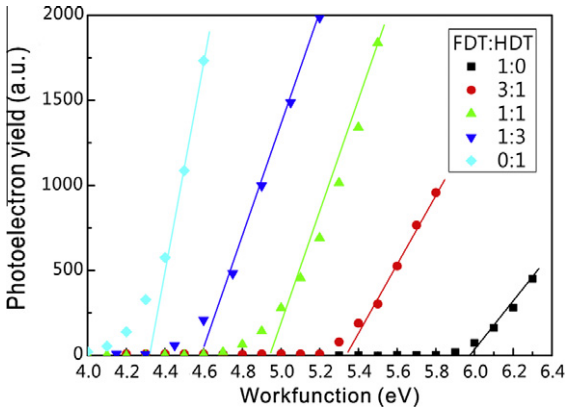

Fig. 1. The work function, measured by photoelectron spectrometer, of silver electrodes modified by various mole ratios of HDT and FDT SAMs.

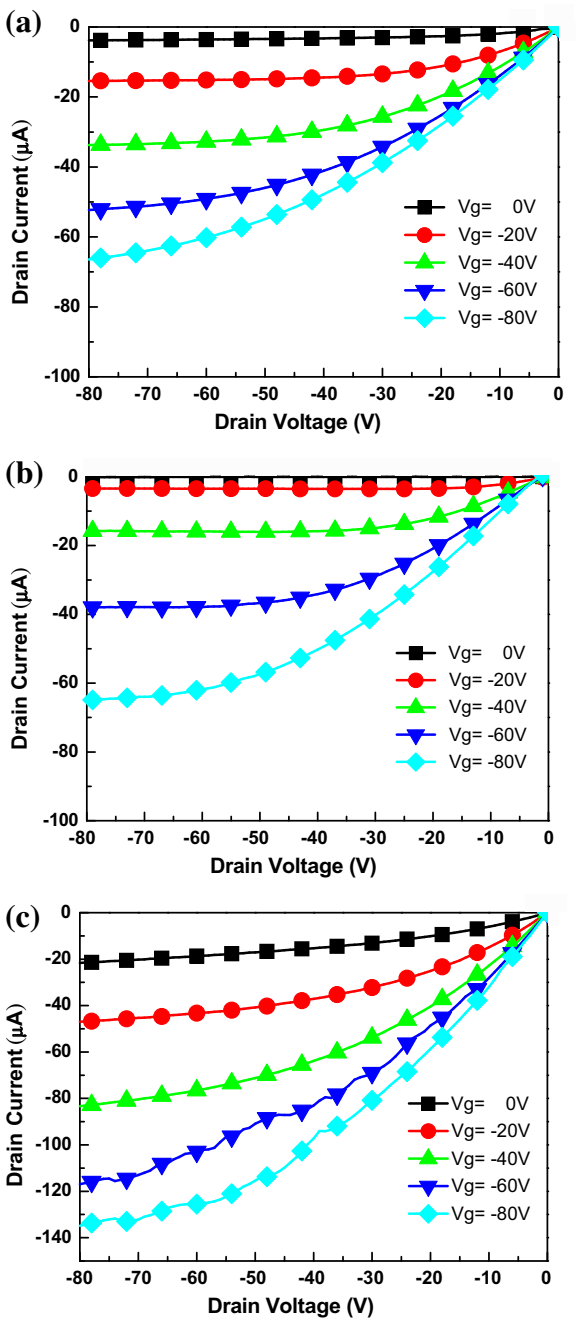

Fig. 2. Drain current–drain voltage characteristics of pentacene-based TFTs with (a) bare gold electrodes, (b) SAM-modified gold electrodes and (c) SAM-modified silver electrodes.

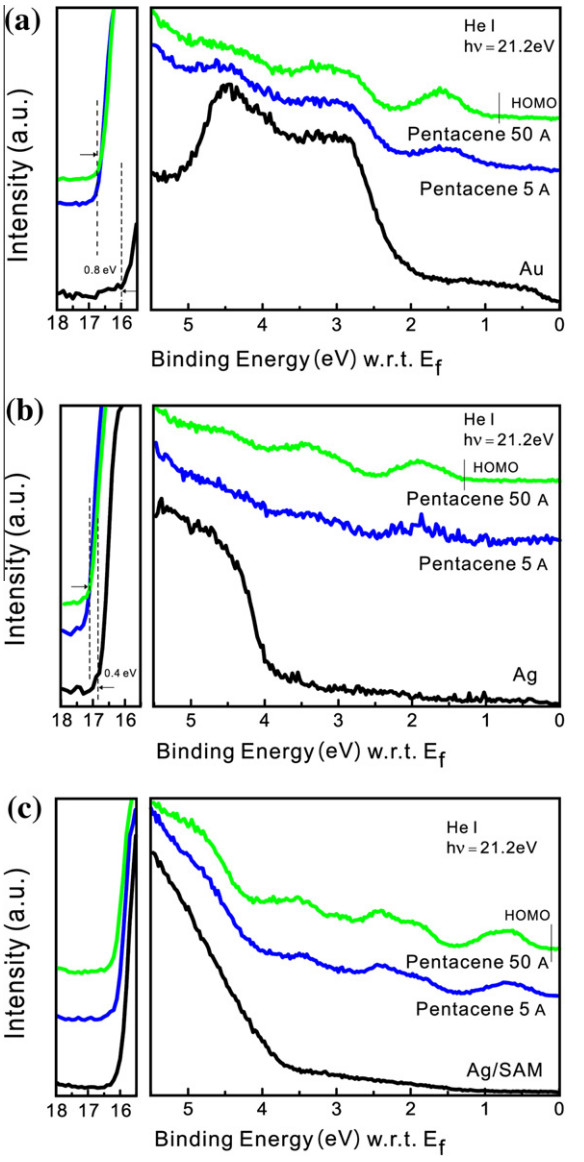

Fig. 3. UPS spectra with incremental deposition of pentacene (a) on gold, (b) on silver, and (c) on SAM-modified silver.

none zero gate voltage (V_G) applied to the transistors. Comparing Fig. 2a–c, when V_G was applied, the devices with silver electrodes modified by FDT and HDT mixtures (the molar ratio of FDT and HDT is 3–1) show better output electrical characteristics as compared to the devices with gold electrodes with or without SAM-modification. The saturation current of devices with SAM-treated Ag electrodes at $V_G = -80$ V reached up to -135 μA, which is two times larger than that with Au electrodes. The carrier mobility at saturation region of devices with Au electrodes is calculated to be 0.08 cm^2/V s from the typical square law of transistor [4,6]. The on–off ratio and threshold voltage is approximately 10^4 and -18 V to -30 V, respectively. For SAM-treated device, the carrier mobility at saturation region is about 0.21 cm^2/V s, which is higher than that of the devices with Au electrodes in this work (0.08 cm^2/V s) and also the similar devices reported from other groups (0.06 cm^2/V s) [24,25]. The on–off ratio and threshold voltage is extracted to be 10^3 and -5.4 V, respectively. The threshold voltage of devices with SAM-modified Ag electrodes is substantially reduced as compared to that of the reference devices with Au electrodes. This threshold voltage shifts toward the positive value are due to the

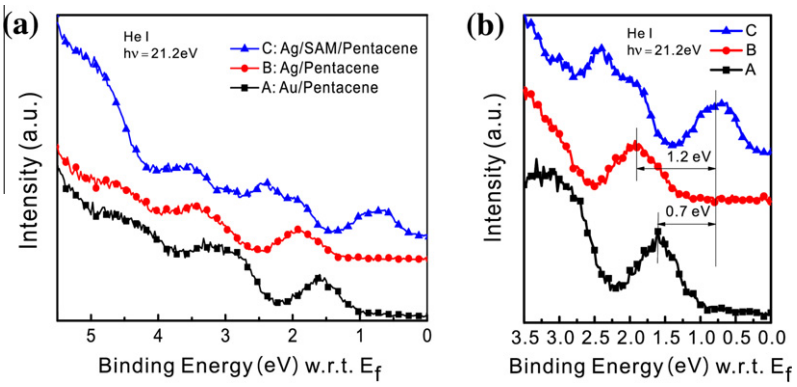

Fig. 4. (a) The valence spectra, of pentacene on gold, silver, and SAM-modified silver, respectively. (b) The magnified spectra of (a), near the E_F and HOMO.

F^- ions at the end of the FDT which induce the holes of pentacene to accumulate at zero gate voltage. As a result, with the negative gate voltage applied, the channel quickly becomes conductive, resulting in the smaller threshold voltage.

UPS with He I (21.2 eV) is used to provide the explicit energy level alignments for metals and organic layers. Fig. 3a–c shows the UPS (He I) spectra for pentacene on the vacuum-deposited gold substrate, on the vacuum-deposited silver substrate, and on the SAM-treated silver substrate, respectively. All the binding energies are with respect to the Fermi level in the spectra. The cut-off binding energy of secondary electrons at the left-hand side of each figure corresponds to the position of the vacuum level. The right-hand side of each figure indicates the relative energy position of the Fermi level (E_F) for each substrate and the highest occupied molecular orbital level (HOMO) for pentacene. In Fig. 3a shows that the vacuum level moves toward the higher binding energy by 0.6 eV as pentacene is deposited on the gold substrate. The valence-band features of gold are still clearly seen in the UPS spectra with 0.5-nm pentacene deposited. As 5-nm pentacene is deposited, the vacuum level shifts by as much as 0.8 eV on the gold substrate and the HOMO of pentacene is clearly observed. The HOMO level of pentacene is about 0.8 eV below the Fermi level as shown in Fig. 3a. Fig. 3b reveals the vacuum level shifts toward higher binding energy by 0.4 eV as pentacene is deposited on the silver surface. For the silver substrate, the edge of the HOMO of pentacene is 1.3 eV below the Fermi level, which is much larger than that of the gold substrate. However, no obvious shift of the vacuum level is observed on the SAM-modified silver as shown in Fig. 3c. In addition, the valence-band features of silver are barely observed in the bottom spectrum of Fig. 3c with the SAM-modified silver, indicating that the silver surfaces are covered well by SAMs.

Fig. 4 combines the valence band spectra of pentacene on these three substrates together for direct comparison. With treatment of mixture-SAMs on silver, the hole injection barrier, i.e. the energy of the HOMO of pentacene with respect to the Fermi level, is remarkably reduced by 1.2 eV as compared to that on pure silver, and is also lower by 0.7 eV as compared to that on gold. The band diagrams, constructed from the valence band spectra, of these three cases are shown in Fig. 5. The measured work functions of gold, silver, and SAM-modified silver are 5.2 eV, 4.3 eV, and 5.1 eV, respectively. In addition, there is little shift of the vacuum level at the interfaces of pentacene/SAM-modified silver, but a vacuum level shift of 0.8 eV on pentacene/gold and of 0.4 eV on pentacene/silver is observed. The large vacuum level shift on gold is typically observed at the initial stage of pentacene deposition [14,26]. The shift of vacuum level is attributed to the interface dipole between the gold and pentacene. However, there is little interface dipole between SAM-modified silver and pentacene, corresponding to minimal shift of the vacuum level. The hole injection barrier is defined as the energy difference of the Fermi level of the substrate and the HOMO of pentacene. As shown in Fig. 5 the hole injection barrier is 0.8 eV for pentacene on gold, 1.3 eV for pentacene on silver, and 0.1 eV for pentacene on SAM-modified silver.

Au with a work function of 5.2 eV, measured in this work, is close to the HOMO level of pentacene (5.1–5.2 eV). The SAM-modified Ag with the work function of 5.1 eV in this work, is also close to the HOMO level of

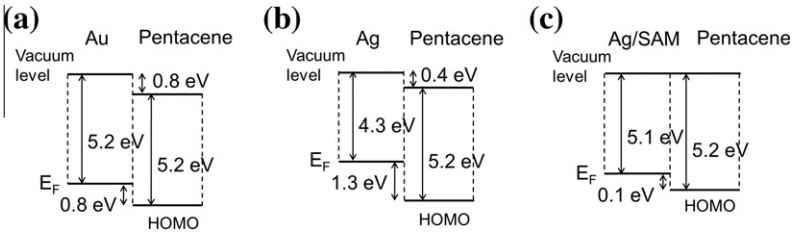

Fig. 5. The energy band diagrams at the interfaces of (a) gold/pentacene. (b) silver/pentacene. (c) SAM-modified silver/pentacene.

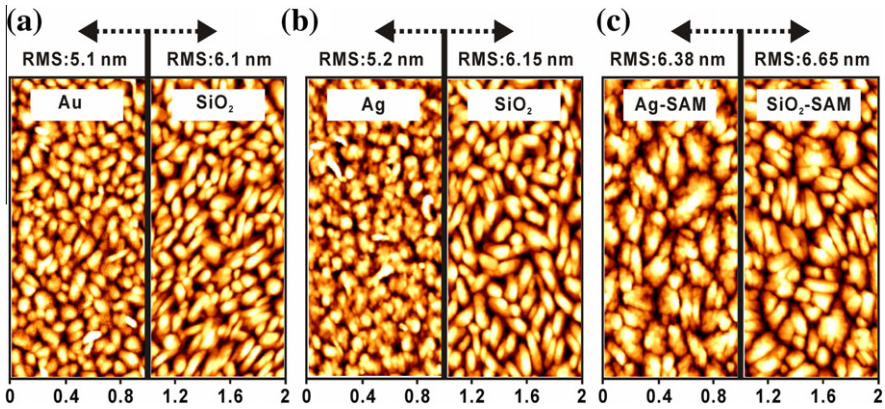

Fig. 6. AFM images of pentacene grown (a) on Au and SiO_2 (b) on Ag and SiO_2 (c) on SAM-modified Ag and SiO_2.

pentacene. Since the work function of these two metals both match the HOMO energy level of pentacene, the drain–source current, I_{DS}, is thought to be similar in the devices with these two electrodes. However, as shown in Fig. 2, the device with SAM-modified Ag electrodes shows a better performance as compared to the Au-electrode device. This is consistent with the hole injection barriers of these electrodes shown in Fig. 4. The device with SAM-modified Ag electrodes has a lower hole injection barrier, around 0.1 eV, than that of the Au-electrode device, which has hole injection barrier of as much as 0.8 eV. The smaller hole injection barrier results in better current injection from the electrodes to pentacene, and thus the better saturation current and mobility of the SAM-modified device. The Ag-electrode device has much higher hole injection barrier of 1.3 eV, and therefore the Ag-electrode device shows no transistor characteristics.

The electrical characteristics of devices are not only affected by the hole injection barrier between electrodes and organic layer. In fact, it is also related to the film morphologies [27–29]. We carried out AFM measurement of pentacene grown on Au, Ag, and SAM-modified Ag to SiO_2, as shown in Fig. 6a–c. Fig. 6a and b shows a relative small pentacene grain size on Au, Ag, and SiO_2. In Fig. 6c, pentacene grains on the SAM-modified Ag devices become larger on modified-Ag electrodes and SiO_2, which would lead to an increase in saturation current and mobility of the devices. Fig. 7a and c shows the AFM images of pentacene

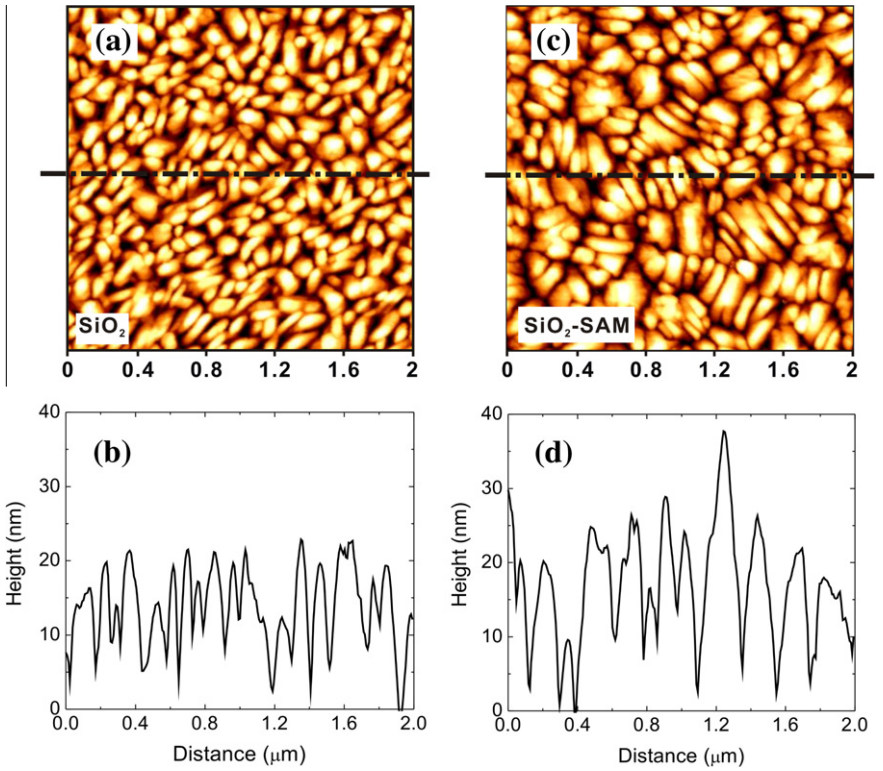

Fig. 7. AFM images of pentacene grown on SiO_2 and SAM-modified SiO_2 and the corresponding line profiles of the images.

grown on SiO_2 and SAM-modified SiO_2, respectively, and the corresponding line profiles are shown as Fig. 7b and d. The results also imply that the FDT-HDT mixed SAMs can modify not only the Ag electrodes, but also change the SiO_2 surfaces at the same time. The mobility and saturation current of Au-electrode devices is not as good as SAM-modified Ag-electrode devices. Therefore, it is evident that both the size of the grain of pentacene and the hole injection barrier between electrodes to organic layers result in the enhance electrical performance of TFTs.

4. Conclusion

In summary, the electrical properties of the organic thin film transistors with SAM-modified Ag electrodes were investigated. The devices with Ag electrodes modified by mixture-SAMs have better saturation current of −135 μA and the mobility of 0.21 cm^2/V s, which are both better than that of the devices with conventional Au electrodes. The hole injection barrier and the pentacene morphology were further investigated by the UPS and AFM. We conclude that the better saturation current and the mobility of the devices are due to the lower hole injection barrier and the large and continuous grain size of pentacene on electrodes.

Acknowledgments

This work was supported by Academia Sinica and the National Science Council (Grant Nos. NSC-98-2112-M-016-MY3 and NSC 100-3113-E-001-001), and "Aim for Top University Project" from the Ministry of Education, Taiwan. The authors would like to thank Mr. H.-H. Wu, Syskey Technology Corp. (Taiwan), for the assistance in fabrication system designed.

References

[1] G. Horowitz, Adv. Mater. 10 (1998) 365–376.
[2] H. Klauk, D.J. Gundlach, J.A. Nichols, T.N. Jackson, IEEE Trans. Electron Device 46 (1999) 1258–1263.
[3] C.D. Dimitrakopoulos, P.R.L. Malenfant, Adv. Mater. 14 (2002) 99–117.
[4] C.D. Sheraw, L. Zhou, J.R. Huang, D.J. Gundlach, T.N. Jackson, Appl. Phys. Lett. 80 (2002) 1088–1090.
[5] A. Dodabalapur, Z. Bao, A. Makhija, J.G. Laquindanum, V.R. Raju, Y. Feng, H.E. Katz, J. Rogers, Appl. Phys. Lett. 73 (1998) 142–144.
[6] S. Steudel, S.D. Vusser, K. Myny, M. Lenes, J. Genoe, P. Heremans, J. Appl. Phys. 95 (2006) 114519.
[7] B. Crone, A. Dodabalapur, A. Gelperin, L. Torsi, H.E. Katz, A.J. Lovinger, Z. Bao, Appl. Phys. Lett. 78 (2001) 2229–2231.
[8] H. Ishii, K. Sugiyama, E. Ito, K. Seki, Adv. Mater. 11 (1999) 605–625.
[9] D. Cahen, A. Kahn, Adv. Mater. 15 (2003) 271–277.
[10] B.H. Hamadani, D. Natelson, J. Appl. Phys. 97 (2005) 064508.
[11] D.J. Gundlach, L. Zhou, J.A. Nichols, T.N. Jackson, P.V. Necliudov, M.S. Shur, J. Appl. Phys. 100 (2006) 024509.
[12] I.G. Hill, D. Milliron, J. Schwartz, A. Kahn, Appl. Surf. Sci. 166 (2000) 354–362.
[13] A. Kahn, N. Koch, W. Gao, J. Polym. Sci. B: Polym. Phys. 41 (2003) 2529–2548.
[14] K. Hong, J.W. Lee, S.Y. Yang, K. Shin, H. Jeon, S.H. Kim, C. Yang, C.E. Park, Org. Electron. 9 (2008) 21–29.
[15] J.P. Hong, A.Y. Park, S. Lee, J. Kang, N. Shin, D.Y. Yoon, Appl. Phys. Lett. 92 (2008) 143311.
[16] K.Y. Wu, S.Y. Yu, Y.T. Tao, Langmuir 25 (11) (2009) 6232–6238.
[17] B. de Boer, A. Hadipour, M.M. Mandoc, T. van Woudenbergh, P.W.M. Blom, Adv. Mater. 17 (2005) 621–625.
[18] C. Bock, D.V. Pham, U. Kunze, D. Kafer, G. Witte, A. Terfort, Appl. Phys. Lett. 91 (2007) 052110.
[19] D. Boudinet, M. Benwadih, Y. Qi, S. Altazin, J.M. Verilhac, M. Kroger, C. Serbutoviez, R. Gwoziecki, R. Coppard, G.L. Blevennec, A. Kahn, G. Horowitz, Org. Electron. 11 (2010) 227–237.
[20] I.H. Campbell, S. Rubin, T.A. Zawodzinski, J.D. Kress, R.L. Martin, D.L. Smith, Phys. Rev. B 54 (1996) 14321–14324.
[21] X. Cheng, Y.Y. Noh, J. Wang, M. Tello, J. Frisch, R.P. Blum, A. Vollmer, J.P. Rabe, N. Koch, H. Sirringhaus, Adv. Funct. Mater. 19 (2009) 2407–2415.
[22] Z. Jia, V.W. Lee, I. Kymissis, L. Floreano, A. Verdini, A. Cossaro, A. Morgante, Phys. Rev. B 82 (2010) 125457.
[23] D.J. Gundlach, J.E. Royer, S.K. Park, S. Surbramanian, O.D. Jurchescu, B.H. Hamadani, A.J. Moad, R.J. Kline, L.C. Teague, O. Kirillov, C.A. Richter, J.G. Kushmerick, L.J. Richter, S.R. Parkin, T.N. Jackson, J. E Anthony, Nat. Mater. 7 (2008) 216–221.
[24] S.W. Liu, C.C. Lee, H.L. Tai, J.M. Wen, J.H. Lee, C.T. Chen, ACS Appl. Mater. Interfaces 2 (8) (2010) 2282–2288.
[25] M. Shtein, J. Mapel, J.B. Benziger, S.R. Forrest, Appl. Phys. Lett. 81 (2) (2002) 268–270.
[26] N.J. Watkins, Q.T. Le, S. Zorba, L. Yan, Y. Gao, S.F. Nelson, C.S. Cuo, T.N. Jackson, Proc. SPIE 4466 (2001) 1.
[27] F. Biscarini, P. Samorí, O. Greco, R. Zamboni, Phys. Rev. Lett. 78 (1997) 2389–2392.
[28] R. Ruiz, B. Nicke, N. Koch, L.C. Feldman, R.F. Haglund, A. Kahn, G. Scoles, Phys. Rev. B 67 (2003) 125406.
[29] R. Hayakawa, M. Petit, Y. Wakayama, T. Chikyow, Org. Electron. 8 (2007) 631–634.